

Quark matter under strong electric fields in the linear sigma model coupled with quarks

William R. Tavares^{1,*}, Sidney S. Avancini^{2,†} and Ricardo L. S. Farias^{3,‡}

¹*Departamento de Física Teórica, Universidade do Estado do Rio de Janeiro, 20550-013 Rio de Janeiro, RJ, Brazil*

²*Departamento de Física, Universidade Federal de Santa Catarina, 88040-900 Florianópolis, SC, Brazil*

³*Departamento de Física, Universidade Federal de Santa Maria, 97105-900 Santa Maria, RS, Brazil*



(Received 18 May 2023; accepted 5 July 2023; published 24 July 2023)

In this work we study the influence of external electric field and temperature on the chiral phase transition of quantum chromodynamics. We use the two-flavor linear sigma model coupled with quarks in a thermal and electrized medium to evaluate the effective quark mass and the Schwinger pair production. To this end, we apply one-loop correction to the fermionic sector of the model and the simple tree-level approximation in the mesonic contributions. The electric fields strengthen the partial restoration of the chiral symmetry when applied with finite temperature in a crossover transition. The expected decrease of the pseudocritical temperature as a function of the electric field is observed until electric fields reach $eE \approx 13.5m_\pi^2$. For stronger electric fields, the effect is the opposite, which is in a very good agreement with previous results obtained with four-point nonrenormalizable models, showing that this effect is independent of renormalizability issues. We also show the thermal and electric effects on the behavior of the Schwinger pair production.

DOI: [10.1103/PhysRevD.108.016017](https://doi.org/10.1103/PhysRevD.108.016017)

I. INTRODUCTION

Experimental efforts over the last few decades can give us very strong evidence of the formation of quark-gluon plasma in the relativistic heavy-ion collisions (HIC) [1–3]. If one assumes basic ideas from classical electromagnetism, one can obtain that strong magnetic fields perpendicular to the reaction plane can be present in peripheral heavy-ion collisions with $eB \sim 10^{19}$ G [4]. This is a preliminary sketch of more sophisticated computational techniques that predict magnetic fields of the same order of magnitude depending on the impact parameter, electrical conductivity, and the collision time [5–7]. Besides that, recent numerical simulations predict that strong magnetic and electric fields should be present in peripheral HIC, which is the case observed in asymmetrical collisions [8–11]. In such situations, e.g., Cu + Au collisions, strong electric fields are expected due to the difference of electric charges in the region where the nuclei overlap. It is also feasible to

anticipate the emergence of strong electric fields by predictions of event-by-event fluctuations of proton position within the colliding nuclei of Au + Au and Pb + Pb [12–15] at the usual collision energy scale $\sqrt{s} = 2.76$ TeV and $\sqrt{s} = 200$ GeV from ALICE and RHIC respectively. Additionally, the presence of electric fields can be very interesting to better understand anomalous transport properties as the chiral separation effect [4,16–18], the chiral magnetic effect [19], and several other quantities in the phase diagram of quantum chromodynamics (QCD).

Despite the numerical evidence about strong electric fields in HIC, there is still little effort to increment QCD phase diagram analysis in such an environment. In lattice QCD, the main reason concerns technical issues similar to the sign problem [20,21] which makes such applications very difficult, regardless of a few recent works with some improvements [21–24]. In this way, the current literature about electric fields in QCD is restricted basically to low energy effective models and some applications in quantum field theories, such as the case of the Nambu–Jona-Lasinio (NJL) model and its extensions [25–31], chiral perturbation theory [32,33], Dyson-Schwinger equations [34,35], and $\lambda\phi^4$ theory [36–38]. Most of these models are in good agreement with regard to the partial restoration of the chiral symmetry guided by electric fields, namely inverse electric catalysis (IEC). In the case of the NJL model, some different regularization techniques have also been used to evaluate not just the behavior of the effective quark mass

*wr.tavares@yahoo.com

†sidney.avancini@ufsc.br

‡ricardo.farias@ufsm.br

Published by the American Physical Society under the terms of the Creative Commons Attribution 4.0 International license. Further distribution of this work must maintain attribution to the author(s) and the published article's title, journal citation, and DOI. Funded by SCOAP³.

but also the Schwinger pair production [27], even in more complex environments including electric fields [28,29]. If simultaneously to the electric fields we include the temperature, the two-flavor NJL [25,26] results indicate that both quantities will strengthen the partial chiral symmetry restoration, with the decreasing of the pseudocritical temperature as a function of the electric fields until $eE \sim 13.5m_\pi^2$, where an opposite behavior is predicted, which until now is due to inconclusive reasons [26]. The same qualitative result has been obtained in the context of the $\lambda\phi^4$ self-interacting scalar field theory [36].

In the present work we explore for the first time, the two-flavor linear sigma model (LSMq) coupled with quarks with a constant electric field and finite temperatures. We apply the one-loop correction in the fermionic sector of the model and the usual tree-level approximation for the mesonic sector. Inspired by the regularized expressions of the pure electric field part in the thermodynamic potential, developed in the context of the NJL model [25,26], we apply these sets of equations in the renormalizable version of LSMq. Our aim is to reanalyze all the basic physics of the model, i.e., effective quark masses, Schwinger pair production, and observe how the pseudocritical temperature for chiral symmetry restoration behaves as a function of the electric fields. These quantities must be enough to know how the renormalizability affects the results in comparison with previous results obtained in the NJL model.

The work is organized in the following structure: In Sec. II we present the formalism details of LSMq including effects of an electric field and finite temperature. In Sec. III we show the equations of the one-loop correction for the fermionic contribution including thermoelectric effects. The numerical results are present in Sec. IV and the conclusions in Sec. V. Appendix A is devoted to the explicit computation of the minimum of the effective potential.

II. LAGRANGIAN OF THE SU(2) LSMq WITH ELECTRIC FIELDS

The Lagrangian of the SU(2) LSMq in an external electromagnetic field is given in Euclidean space by the following expression [39]:

$$\mathcal{L} = \bar{\psi}[i\not{D} + g(\sigma + i\gamma_5\vec{\tau} \cdot \vec{\pi})]\psi + \frac{1}{2}[(\partial_\mu\sigma)^2 + (\partial_\mu\vec{\pi})^2] + U(\sigma, \vec{\pi}) - \frac{1}{4}F_{\mu\nu}F_{\mu\nu}, \quad (1)$$

where A_μ and $F_{\mu\nu} = \partial_\mu A_\nu - \partial_\nu A_\mu$ are respectively the electromagnetic gauge and tensor fields, g is the Yukawa coupling constant, $\vec{\tau}$ are isospin Pauli matrices, Q is the diagonal quark charge¹ matrix,

¹Our results are expressed in Gaussian natural units where $1 \text{ GeV}^2 = 1.44 \times 10^{19} G$ and $e = 1/\sqrt{137}$.

$Q = \text{diag}(q_u = 2/3, q_d = -1/3)$, $D_\mu = (\partial_\mu + ieQA_\mu)$ is the covariant derivative, and we adopt $A_\mu = -\delta_{\mu 4}x_3E$ in order to include in the z direction a constant electric field. In this model, we have the following quantum fields: $\psi = (\psi_u\psi_d)^T$ which are the quark fermion fields and the mesonic degrees of freedom as given by the σ and $\vec{\pi}$ fields. The purely mesonic potential, $U(\sigma, \vec{\pi})$, in Eq. (1), is given by

$$U(\sigma, \vec{\pi}) = \frac{1}{2}m^2(\sigma^2 + \vec{\pi}^2) + \frac{\lambda}{24}(\sigma^2 + \vec{\pi}^2)^2 - h\sigma, \quad (2)$$

where λ, m^2 and h are constants fixed by experimental parameters as the σ and π meson masses and the pion decay constant, f_π . The value of $h = f_\pi m_\pi^2$ ensures the explicit breaking of the chiral symmetry, i.e., the $SU(2)_v$ group. We adopt, for simplicity the mean field values of $\langle\sigma\rangle \equiv \phi$ and $\langle\vec{\pi}\rangle \equiv \vec{\pi} = 0$.

The tree-level effective potential in a constant electric field for the LSMq is given by

$$F^0 = U(\phi, \vec{\pi}) - \frac{1}{4}E^2; \quad (3)$$

this representation is useful for making clear some of our renormalization procedures to the one-loop fermionic correction to the effective potential.

The meson and quark masses, at the tree-level approximation, are given by [39]

$$m_\sigma^2 = m^2 + \frac{\lambda}{2}\phi^2, \quad (4)$$

$$m_\pi^2 = m^2 + \frac{\lambda}{6}\phi^2, \quad (5)$$

$$M = g\phi, \quad (6)$$

where ϕ is the vacuum expectation value of the σ field.

III. ONE-LOOP FERMIONIC CONTRIBUTION

In this work we treat the mesonic sector at tree level and include quantum corrections only in the fermionic sector. The one-loop correction to the fermionic contributions at $eE = T = 0$ is given by [40–43]

$$F_{\text{vac}}^1 = -2N_c N_f \int \frac{d^4 p}{(2\pi)^4} \log(p_0^2 + E_p^2) + C, \quad (7)$$

where C is a mass-independent constant that can be ignored, and N_c and N_f are the number of colors and flavors, respectively. The energy dispersion relation, E_p , is given by

$$E_p^2 = M^2 + p^2. \quad (8)$$

In the $\overline{\text{MS}}$ scheme [39], we obtain for Eq. (7) the following expression:

$$F_{\text{vac}}^1 = \frac{N_c N_f M^4}{16\pi^2} \left[\log\left(\frac{\Lambda^2}{M^2}\right) + \frac{3}{2} \right], \quad (9)$$

where Λ is the renormalization scale. In the present scheme, one needs to include the counterterms $m^2 \rightarrow m^2 + \Delta m^2$ and $\lambda \rightarrow \lambda + \Delta\lambda$ [39], where

$$\Delta m^2 = \frac{\lambda m^2}{16\pi^2 \epsilon}, \quad (10)$$

$$\Delta\lambda = \frac{2\lambda^2 - 24N_c N_f g^4}{16\pi^2 \epsilon} \quad (11)$$

$$\delta\epsilon = \frac{m^4}{16\pi^2 \epsilon}, \quad (12)$$

where we have included a vacuum energy counterterm $\Delta\epsilon$ [39].

When considering a constant electric field, the one-loop fermion contribution can be written in the proper-time formalism [44]

$$F^1(\mathcal{E}, M) = \sum_f \frac{N_c}{8\pi^2} \int_0^\infty ds \frac{e^{-sM^2}}{s^2} \mathcal{E}_f \cot(\mathcal{E}_f s), \quad (13)$$

where $\mathcal{E}_f = |q_f eE|$. We can verify the validity of the last expression by evaluating the analytic extension derived by Schwinger [44], i.e., $eE \rightarrow ieB$, where we obtain the exact expression to the LSMq with a constant magnetic field in the z direction [25,26].

The integration in Eq. (13) has divergences with different sources. First, we treat the divergence in the lower limit of integration, $s = 0$, by using the separation of divergences from Schwinger's work in QED [44]. For this purpose we use the Taylor expansion of the $\cot(\mathcal{E}_f s)$ function for $\mathcal{E}_f s \ll 1$:

$$\cot(\mathcal{E}_f s) \sim \frac{1}{\mathcal{E}_f s} - \frac{\mathcal{E}_f s}{3} - \frac{(\mathcal{E}_f s)^3}{45} + \mathcal{O}((\mathcal{E}_f s)^5), \quad \mathcal{E}_f s \ll 1.$$

Using the expansion in Eq. (13), we can avoid the divergences in the region $s = 0$:

$$\begin{aligned} F^1(\mathcal{E}, M) &= \sum_f \frac{N_c}{8\pi^2} \int_0^\infty ds \frac{e^{-sM^2}}{s^3} \left(\mathcal{E}_f s \cot(\mathcal{E}_f s) - 1 \right. \\ &\quad \left. + \frac{(\mathcal{E}_f s)^2}{3} \right) + \frac{N_c}{8\pi^2} \sum_f \int_{\frac{1}{\Lambda^2}}^\infty ds \frac{e^{-sM^2}}{s^3} \\ &\quad - \frac{N_c}{24\pi^2} \sum_f \mathcal{E}_f^2 \int_{\frac{1}{\Lambda^2}}^\infty ds \frac{e^{-sM^2}}{s}. \end{aligned} \quad (14)$$

In Eq. (14) the first three terms are the finite electric field contributions, which were regularized with respect to the ultraviolet divergence from the contributions near $s = 0$. In the second term of the second line, we have the fermionic contribution from the vacuum given in Eq. (9) and the field contribution, proportional to \mathcal{E}^2 , that must be regularized and renormalized. For simplicity, we define the one-loop fermionic contribution as

$$F^1(\mathcal{E}, M) = F_{\text{vac}}^1(M) + F_{\text{med}}^1(\mathcal{E}, M) + F_{\text{field}}^1(\mathcal{E}, M),$$

where we have separated F^1 in the vacuum, medium, and field contributions. Each term is given by the following expressions:

$$\begin{aligned} F_{\text{med}}^1(\mathcal{E}, M) &= \sum_f \frac{N_c}{8\pi^2} \int_0^\infty ds \frac{e^{-sM^2}}{s^3} \\ &\quad \times \left(\mathcal{E}_f s \cot(\mathcal{E}_f s) - 1 + \frac{(\mathcal{E}_f s)^2}{3} \right), \end{aligned} \quad (15)$$

$$\begin{aligned} F_{\text{vac}}^1(M) &= \frac{N_c}{8\pi^2} \sum_f \int_{\frac{1}{\Lambda^2}}^\infty ds \frac{e^{-sM^2}}{s^3}, \\ &= \frac{N_c N_f M^4}{16\pi^2} \left[\log\left(\frac{\Lambda^2}{M^2}\right) + \frac{3}{2} \right], \end{aligned} \quad (16)$$

$$\begin{aligned} F_{\text{field}}^1(\mathcal{E}, M) &= -\frac{N_c}{24\pi^2} \sum_f \mathcal{E}_f^2 \int_{\frac{1}{\Lambda^2}}^\infty ds \frac{e^{-sM^2}}{s} \\ &= -\frac{N_c}{24\pi^2} \sum_f \mathcal{E}_f^2 \left[-\log\left(\frac{M^2}{\Lambda^2}\right) - \gamma_E + \mathcal{O}\left(\frac{M^2}{\Lambda^2}\right) \right], \end{aligned} \quad (17)$$

where γ_E is the Euler-Mascheroni constant. Usually, the divergence proportional to E^2 is renormalized and incorporated in the $\frac{1}{2}E^2$ from the Lagrangian Eq. (1). For renormalization purposes, we set $E^2 \rightarrow Z^2 E^2$, where

$$Z^2 = \left[1 + N_c \sum_f \frac{4q_f^2}{3(4\pi)^2 \epsilon} \right]. \quad (18)$$

The details of the last contribution are evaluated in Ref. [39], in the case of a constant magnetic field, but in our case we do not consider the one-loop mesonic contributions.

Now we work with the divergent contributions present in Eq. (15), that occurs in the proper-time integration when $\mathcal{E}_f s = n\pi$ in the cotangent function, with $n = 0, 1, 2, 3, \dots$. These divergences are associated with the instabilities in the vacuum due to the electric field, which gives rise to the Schwinger pair production of quarks. We extend analytically to the complex plane the integration and separate the

real from the imaginary part. This procedure is developed in detail in Ref. [25]. This gives rise to the following result:

$$\Re(F_{\text{med}}^1(\mathcal{E}, M)) = \frac{N_c}{2\pi^2} (\mathcal{E}_f)^2 \left\{ \zeta'(-1) + \frac{\pi}{4} y_f + \frac{y_f^2}{2} \times \left(\gamma_E - \frac{3}{2} + \ln y_f \right) - \frac{1}{12} (1 + \ln y_f) + \sum_{k=1}^{\infty} k \left[\frac{y_f}{k} \tan^{-1} \left(\frac{y_f}{k} \right) - \frac{1}{2} \ln \left(1 + \left(\frac{y_f}{k} \right)^2 \right) - \frac{1}{2} \left(\frac{y_f}{k} \right)^2 \right] \right\}, \quad (19)$$

where $y_f = \frac{M^2}{2\mathcal{E}_f}$ and $\zeta'(-1) = 1/2 - \log(A)$ with $A = 1.282417\dots$ being the Gleisher-Kinkelin constant [45]. The imaginary part of the one-loop effective potential is

$$\Im(F^1(\mathcal{E}, M)) = -\frac{N_c}{8\pi} \sum_f \mathcal{E}_f^2 \sum_{k=1}^{\infty} \frac{e^{-\frac{M^2 \pi k}{\mathcal{E}_f}}}{(k\pi)^2}. \quad (20)$$

The thermoelectric contribution, derived in Appendix B, is evaluated in the imaginary-time formalism. The result is given by

$$\Re(F_{\text{therm}}^1(\mathcal{E}, M, T)) = -\frac{N_c}{2\pi^2} \sum_{n=1}^{\infty} (-1)^n \mathcal{E}_f \int_0^{\infty} ds \frac{e^{-sM^2}}{s} \times \cot(\mathcal{E}_f s) e^{-\frac{\mathcal{E}_f n^2}{4|\tan(\mathcal{E}_f s)|T^2}}, \quad (21)$$

where the summation is over the Matsubara frequencies. The thermoelectric contribution is finite due to the Fermi-Dirac distribution, written in the proper-time formalism. The full thermodynamic potential, including the tree-level potential F^0 in Eq. (3), is given, therefore, by

$$\Re(F(\mathcal{E}, M, T)) = \Re(F^0 + F^1(\mathcal{E}, M) + F_{\text{therm}}^1(\mathcal{E}, M, T)). \quad (22)$$

It is possible to show that, given the thermodynamic potential, we can derive the Schwinger pair production rate, i.e., $\Gamma(\mathcal{E}, T, M) = -2\Im(F^1(\mathcal{E}, M, T))$ [25,26].

In order to fix Λ , at $\mathcal{E} = T = 0$, we choose the physical point $\phi = f_\pi$, which configures the partially conserved axial vector current relation in this model, at the minimum of the effective potential [39], i.e.,

$$\left. \frac{d(\Re F(\mathcal{E}, M, T))}{d\phi} \right|_{\phi=f_\pi} = 0. \quad (23)$$

To obtain the behavior of the effective quark mass as a function of the temperature and electric fields, we evaluate the gap equation, given in Appendix A.

IV. NUMERICAL RESULTS

In this section we present and discuss our numerical results. The model requires fixing three independent parameters: the mass parameter m , the boson-fermion coupling g , and the boson self-coupling λ . These parameters are fixed in such a way to obtain with LSMq the vacuum values of pion mass, $m_\pi = 140$ MeV; pion decay constant, $f_\pi = 93$ MeV; the σ meson mass, $m_\sigma = 800$ MeV; and effective quark masses $M = 300$ MeV [39]. The σ meson mass is chosen at the upper end of the state $f_0(500)$ [46]. With these experimental inputs, we obtain the following set of parameters: $g = 3.2258$, $m^2 = -290600$ MeV², and $\lambda = 215.19$. We also need to fix the renormalization scale Λ . Once we have determined the parameters m , g , and λ we can choose the value of Λ where the minimum of the one-loop effective potential in the vacuum remains the same at tree-level value ($\phi = 93$ MeV). A similar procedure was made in [39], and the value obtained for the renormalization scale was $\Lambda = 181.96$ MeV.

In Fig. 1 we can see the effective quark mass as a function of the temperature for different values of electric fields. For low values of electric fields, we can see the partial restoration of chiral symmetry as we increase the temperature. This effect is strengthened for higher values of electric fields, which is very clear for strong enough values, e.g., $eE = 15m_\pi^2$ and $eE = 18m_\pi^2$. Additionally, for all of these cases, the transition is a crossover. Although the two effects combine themselves to partially restore the chiral symmetry, they are different physical phenomena, i.e., the temperature excites the system weakening the interaction in the chiral condensate. On the other hand, the electric fields accelerate the charges with different signs in opposite directions, inducing the chiral condensate to be less likely to happen as we increase the strength of the electric field.

When we increase the electric fields, the transition occurs to lower values of temperatures, indicating IEC of the pseudocritical temperature. However, in the purple dotted line, for $eE = 18m_\pi^2$, we cannot distinguish by Fig. 1

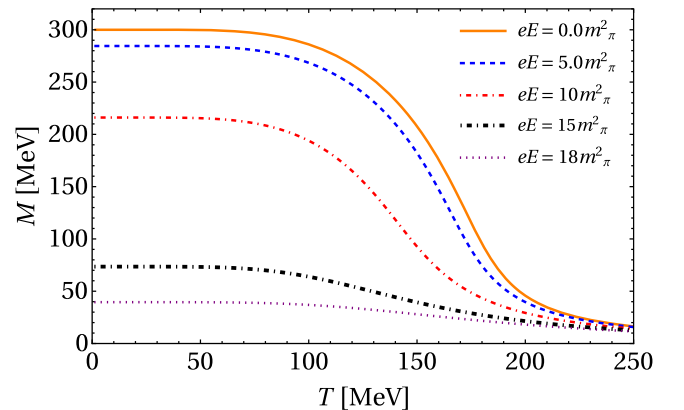


FIG. 1. Effective quark mass as a function of the temperature for different values of electric fields.

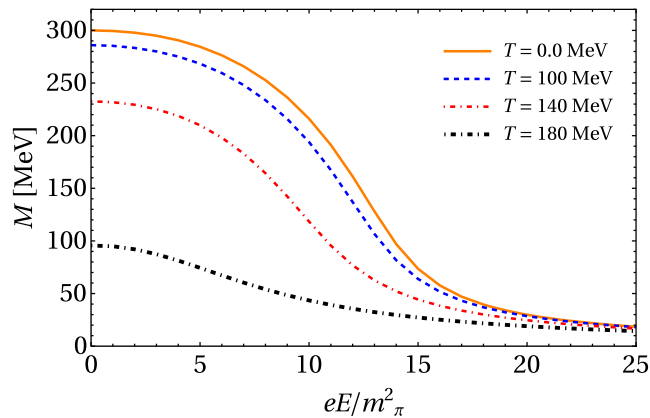


FIG. 2. Effective quark mass as a function of the electric field for different values of temperature.

in a very clear way if we have electric catalysis (EC) or IEC. The phenomena EC and IEC will be easier to verify when we plot the pseudocritical temperature as a function of the electric field.

We can see the effective quark masses as a function of the electric fields for different values of temperature in Fig. 2. The analysis indicates that, at low temperatures, the electric fields partially restore the chiral symmetry breaking at $eE \gg 15m_\pi^2$ as indicated previously in Fig. 1. For low values of the electric fields, we can see the influence of the thermal effects on the partial restoration of the chiral symmetry. On the other hand, as we increase the strength of the electric field, Fig. 2 shows the effect of the electric field on the partial restoration of the chiral symmetry.

In Fig. 3, we show the pseudocritical temperature for chiral symmetry restoration as a function of the electric field. The pseudocritical temperature is calculated as the maximum of the $-\partial M/\partial T$. We can clearly see the IEC effect, which turns into EC for very high values of electric fields, i.e., $eE > 13.5m_\pi^2$, where we have the increasing of

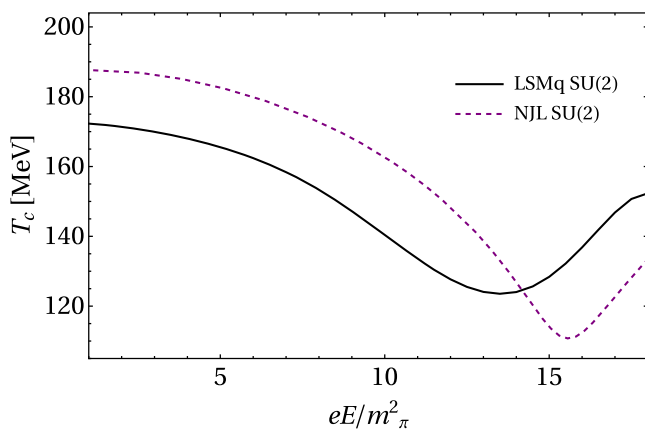


FIG. 3. The pseudocritical temperature for chiral symmetry restoration as a function of the electric field in the LSMq (solid line) and NJL SU(2) (dashed line) [26].

the pseudocritical temperature as a function of the electric fields. This result is in good qualitative agreement with the previous works with SU(2) NJL and Polyakov–Nambu–Jona-Lasinio (PNJL) models [26]. Therefore, the phenomenon observed previously in both NJL and PNJL that the IEC change to EC after a critical value of the electric field cannot be attributed to the regularization issues, which are inherent to nonrenormalizable models. As our results now show, using a renormalizable model one obtains, qualitatively, the same behavior that was previously observed in the NJL and PNJL models. We also would like to mention that, this result is important to guide our comprehension of the effects of electric fields in peripheral HIC, since we are considering constant electric fields. More realistic scenarios with time-dependent electric fields must be explored in the near future. However, numerical simulations with event-by-event fluctuations provide enough results to support that electric fields can be present in the late stages of the formation of quark-gluon plasma [13]. Once the spectators are far away from the collision, the remnants become the source of electromagnetic fields. At this point, the high electric conductivity of the medium plays an important role in delaying the suppression of electromagnetic fields [4,47]. Such a scenario would lead to a decreasing value of the pseudocritical temperature as a function of the electric fields.

The Schwinger pair production as a function of the temperature is given in Fig. 4. We can see that, for lower values of electric fields, e.g., $eE = 5m_\pi^2$, the production is almost zero in the low-temperature limit, and slightly changes at $T > T_{pc}$, indicating that the high temperatures can strengthen the pair production in an electric medium. As we increase the electric fields, the pair production grows in the low-temperature region and substantially increases after the pseudocritical temperature, which we can see in the situations $eE = 10m_\pi^2$ and $eE = 15m_\pi^2$. At very high electric fields, the Schwinger pair production almost does not change in the full temperature range considered.

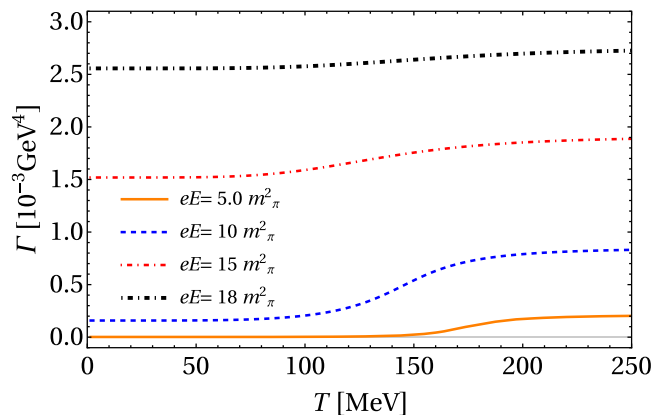


FIG. 4. The Schwinger pair production of quarks as a function of the temperature for different values of the electric fields.

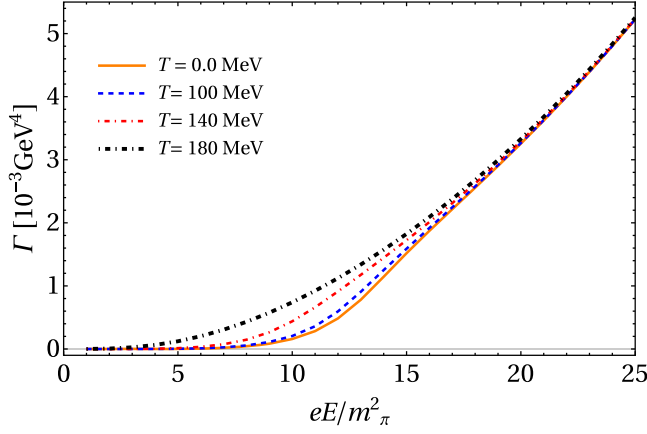


FIG. 5. The Schwinger pair production of quarks as a function of the electric fields for different values of the temperature.

These results are in good agreement with the previous two-flavor NJL model results [25,26].

In Fig. 5 are shown our results for the Schwinger pair production as a function of the electric field normalized by the pion mass squared. It is clear from this figure that non-negligible effects start to appear around $eE = 5m_\pi^2$ and for fixed electric fields the temperature enhances the pair production. Above $eE = 18m_\pi^2$ the pair production saturates. Again, these results are in qualitative agreement with previous NJL and PNJL calculations.

V. CONCLUSIONS

In this work, we have studied within the linear sigma model with quarks, the quark matter at finite temperature with a background of electric fields. One of the main motivations of this study was the estimation of the effects of the strong electric fields on the chiral symmetry restoration scenario within a renormalizable model, and performing the comparison with previous results obtained in SU(2) versions of NJL and PNJL models [26].

Our numerical results have shown that the constituent quark masses decrease when we increase the strength of the electric fields, as a signature of the partial restoration of the chiral symmetry. We have computed the evolution of the pseudocritical temperature for chiral symmetry restoration T_{pc} as a function of the electric fields. In the literature, as expected, usually the pseudocritical temperature for chiral symmetry restoration decreases as we increase the electric field strength. In [26] within the SU(2) PNJL model we have shown, for the first time in the literature, a very interesting effect where for strong enough electric fields the pseudocritical temperature for chiral symmetry restoration starts to increase after a critical value of the electric field. This effect was founded also within LSMq and also propagates to all quantities, as to the Schwinger pair production. In the context of $\lambda\phi^4$ theory similar results were found, which show IEC for weak electric fields and EC for strong electric

field strength [36]. Our work provides strong evidence that the nonmonotonic behavior of the pseudocritical temperature of chiral symmetry restoration as a function of the electric field is a characteristic of QCD, regardless of whether we are working with a renormalizable or non-renormalizable effective model of QCD.

An improvement of the present work is the study of the inclusion of baryon density effects in the presence of thermal and background electric fields. We are currently exploring these avenues in PNJL and LSMq and will report on the findings elsewhere in the near future.

ACKNOWLEDGMENTS

This work was partially supported by Conselho Nacional de Desenvolvimento Científico e Tecnológico (CNPq), 309598/2020-6 (R. L. S. F.), 304518/2019-0 (S. S. A.), 309262/2019-4; Fundação Carlos Chagas Filho de Amparo à Pesquisa do Estado do Rio de Janeiro (FAPERJ), Grant No. SEI-260003/019544/2022 (W. R. T); Fundação de Amparo à Pesquisa do Estado do Rio Grande do Sul (FAPERGS), Grants No. 19/2551-0000690-0 and No. 19/2551-0001948-3 (R. L. S. F.). The work is also part of the project Instituto Nacional de Ciência e Tecnologia—Física Nuclear e Aplicações (INCT—FNA), Grant No. 464898/2014-5.

APPENDIX A: GAP EQUATION

In this section, we will deal with the derivative of the real part of the effective potential. For simplicity, we will define $\Re(F) \equiv F$. The minimum of the effective potential is given by $dF/d\phi = 0$, where $M = g\phi$, as follows:

$$\frac{dF^0}{d\phi} + \frac{dF_{\text{vac}}^1(M)}{d\phi} + \frac{dF_{\text{med}}^1(\mathcal{E}, M)}{d\phi} + \frac{dF_{\text{field}}^1(\mathcal{E}, M)}{d\phi} + \frac{dF_{\text{therm}}^1(\mathcal{E}, M, T)}{d\phi} = 0, \quad (\text{A1})$$

where the first term in Eq. (A1) concerns the tree-level potential, which gives

$$\begin{aligned} \frac{dF^0}{d\phi} &= \frac{dU(\phi, \vec{\pi})}{d\phi} \\ &= m^2\phi + \frac{\lambda}{6}[\phi^2 + \vec{\pi}^2]\phi - h \\ &= m^2\phi + \frac{\lambda}{6}\phi^3 - h, \end{aligned}$$

where we assume that the mean field value $\vec{\pi} \rightarrow \langle \vec{\pi} \rangle = 0$. The second term in Eq. (A1) is the one-loop correction to the fermionic contribution, given by

$$\frac{dF_{\text{vac}}^1(M)}{d\phi} = \frac{N_c N_f g M^3}{4\pi^2} \left[\log\left(\frac{\Lambda^2}{M^2}\right) + \frac{3}{2} \right] - \frac{N_c N_f g M^3}{8\pi^2}. \quad (\text{A2})$$

The medium and field contributions combine themselves as

$$\begin{aligned}
 & \frac{dF_{\text{med}}^1(\mathcal{E}, M)}{d\phi} + \frac{dF_{\text{field}}^1(\mathcal{E}, M)}{d\phi} \\
 &= -\sum_f \frac{gMN_c}{4\pi^2} \int_0^\infty ds \frac{e^{-sM^2}}{s^2} [\mathcal{E}_f s \cot(\mathcal{E}_f s) - 1] \\
 &= \sum_f \frac{gMN_c}{2\pi^2} \mathcal{E}_f \left[\frac{\pi}{4} + y_f(\gamma_E - 1 + \ln y_f) \right. \\
 & \quad \left. + \sum_{k=1}^{\infty} \left(\tan^{-1} \frac{y_f}{k} - \frac{y_f}{k} \right) \right]. \quad (\text{A3})
 \end{aligned}$$

The last term in Eq. (A1) concerns the one-loop thermoelectrical contribution, which is given by

$$\begin{aligned}
 \frac{dF_{\text{therm}}^1(\mathcal{E}, M, T)}{d\phi} &= -\frac{gMN_c}{2\pi^2} \sum_{n=1}^{\infty} (-1)^n \int_0^\infty ds \frac{e^{-sM^2}}{s} \mathcal{E}_f \\
 & \quad \times \cot(\mathcal{E}_f s) e^{\frac{\mathcal{E}_f n^2}{4|\tan(\mathcal{E}_f s)|T^2}}. \quad (\text{A4})
 \end{aligned}$$

Therefore, we obtain the gap equation for numerical analysis.

APPENDIX B: THE THERMOELECTRIC CONTRIBUTION TO $F^1(\mathcal{E}, T, M)$

We present here the main steps to obtain Eq. (21). To this end, we start with the gap equation, and then by integrating with respect to ϕ , we obtain $F^1(\mathcal{E}, T, M)$. At $\mathcal{E} = T = 0$, one can derive the gap equation Eq. (A1), in a very similar fashion as obtained in [48], which reads as

$$\frac{dF^0}{d\phi} + \frac{dF^1}{d\phi} = 0, \quad (\text{B1})$$

$$\frac{dF^1}{d\phi} = gN_c \sum_f \frac{1}{\beta} \sum_{n=-\infty}^{\infty} \int \frac{d^3p}{(2\pi)^3} \text{tr} S_f(\omega_n, \vec{p}), \quad (\text{B2})$$

where $\omega_n = (2n+1)\pi T$, n are the Matsubara frequencies, $\beta = \frac{1}{T}$, $S_f(p)$ is the quark propagator in the momentum space, and the trace is given in the Dirac basis. When considering quarks in an electric field medium, we can use the quark propagator given in Eq. (16) of

Ref. [27] in the limit $B \rightarrow 0$, which has the following structure:

$$\begin{aligned}
 iS_f(p) &= \int_0^\infty ds \exp[-isM^2 - iA(\mathcal{E}_f, s)p_{\parallel}^2 - is p_{\perp}^2] \\
 & \quad \times \Pi(p, \mathcal{E}_f, s). \quad (\text{B3})
 \end{aligned}$$

In the last expression $p_{\parallel}^2 = \omega_n^2 + p_3^2$, $p_{\perp}^2 = p_1^2 + p_2^2$, $A(\mathcal{E}_f, s) = \frac{\tanh(\mathcal{E}_f s)}{\mathcal{E}_f}$, and $\Pi(p, \mathcal{E}_f, s)$ is a function of 4-momenta, electric field, and it possesses a linear dependence on the γ^μ matrices, which leads to the simple result after the calculation of the trace

$$\text{tr} \Pi(p, \mathcal{E}_f, s) = 4M. \quad (\text{B4})$$

The next step involves taking $s \rightarrow -is$, and evaluating Gaussian integrations in p_{\perp} and p_3 , as given in Eq. (B2), which results in

$$\frac{dF^1}{d\phi} = -\frac{MgN_c}{2\pi^2} \sum_f \int_0^\infty ds \frac{e^{-sM^2}}{s} \sqrt{\frac{\pi}{\tilde{A}\tilde{\beta}}} \sum_{n=-\infty}^{\infty} e^{-\tilde{A}\omega_n^2}; \quad (\text{B5})$$

in the last expression $\tilde{A}(\mathcal{E}_f, s) = \frac{\tan(\mathcal{E}_f s)}{\mathcal{E}_f}$. At this point, the evaluation is quite similar to the case of finite magnetic fields explored in Ref. [49]. We can now rewrite the Matsubara sum in Eq. (B5) as,

$$\sum_{n=-\infty}^{\infty} e^{-\tilde{A}\omega_n^2} = e^{-\pi^2 \tilde{A} T^2} \vartheta_3(2\pi i \tilde{A} T^2, 4\pi i \tilde{A} T^2), \quad (\text{B6})$$

where, by definition

$$\vartheta_3(z, x) = \sum_{n=-\infty}^{\infty} e^{i\pi x n^2 + 2i\pi z n} \quad (\text{B7})$$

is the Jacobi $\vartheta_3(z, x)$ function. Now making use of the inversion formula

$$\vartheta_3(z, x) = \sqrt{\frac{i}{x}} e^{\frac{z^2}{ix}} \vartheta_3\left(\frac{z}{x}, -\frac{1}{x}\right), \quad (\text{B8})$$

and identifying $z = \frac{1}{2}$ and $x = \frac{i}{4\pi \tilde{A} T^2}$, we obtain

$$\begin{aligned}
 \frac{dF^1}{d\phi} &= -\frac{MgN_c}{4\pi^2} \sum_f \int_0^\infty ds \frac{e^{-sM^2}}{s} \mathcal{E}_f \cot(\mathcal{E}_f s) \\
 & \quad \times \vartheta_3\left(\frac{1}{2}, \frac{i}{4\pi \tilde{A} T^2}\right). \quad (\text{B9})
 \end{aligned}$$

Now, using the following identity,

$$\vartheta_3\left(\frac{1}{2}, \frac{i}{4\pi\tilde{A}T^2}\right) = 1 + 2 \sum_{n=1}^{\infty} (-1)^n e^{-\frac{\mathcal{E}_f n^2}{4|\tan(\mathcal{E}_f s)|T^2}}, \quad (\text{B10})$$

we can obtain exactly the electric (not regularized) and thermoelectric contributions given in Eq. (A1), i.e.,

$$\frac{dF^1}{d\phi} = -\frac{MgN_c}{4\pi^2} \sum_f \int_0^\infty ds \frac{e^{-sM^2}}{s} \mathcal{E}_f \cot(\mathcal{E}_f s) - \frac{MgN_c}{2\pi^2} \sum_f \int_0^\infty ds \frac{e^{-sM^2}}{s} \mathcal{E}_f \cot(\mathcal{E}_f s) \sum_{n=1}^{\infty} (-1)^n e^{-\frac{\mathcal{E}_f n^2}{4|\tan(\mathcal{E}_f s)|T^2}}. \quad (\text{B11})$$

By a simple integration in ϕ , and ignoring an irrelevant constant of integration, we can achieve $F^1(\mathcal{E}, T, M)$. The real value in Eq. (21) is obtained by numerical evaluation and, for this expression, $\Re(F^1(\mathcal{E}, T, M)) \equiv F^1(\mathcal{E}, T, M)$.

-
- [1] W. Busza, K. Rajagopal, and W. van der Schee, *Annu. Rev. Nucl. Part. Sci.* **68**, 339 (2018).
- [2] H. Elfner and B. Müller, arXiv:2210.12056.
- [3] R. Snellings, *New J. Phys.* **13**, 055008 (2011).
- [4] X. G. Huang, *Rep. Prog. Phys.* **79**, 076302 (2016).
- [5] K. Tuchin, *Phys. Rev. C* **88**, 024911 (2013).
- [6] K. Tuchin, *Phys. Rev. C* **93**, 014905 (2016).
- [7] L. McLerran and V. Skokov, *Nucl. Phys.* **A929**, 184 (2014).
- [8] W. T. Deng and X. G. Huang, *Phys. Lett. B* **742**, 296 (2015).
- [9] Y. Hirono, M. Hongo, and T. Hirano, *Phys. Rev. C* **90**, 021903 (2014).
- [10] V. Voronyuk, V. D. Toneev, S. A. Voloshin, and W. Cassing, *Phys. Rev. C* **90**, 064903 (2014).
- [11] Y. L. Cheng, S. Zhang, Y. G. Ma, J. H. Chen, and C. Zhong, *Phys. Rev. C* **99**, 054906 (2019).
- [12] A. Bzdak and V. Skokov, *Phys. Lett. B* **710**, 171 (2012).
- [13] W. T. Deng and X. G. Huang, *Phys. Rev. C* **85**, 044907 (2012).
- [14] J. Błoczyński, X. G. Huang, X. Zhang, and J. Liao, *Phys. Lett. B* **718**, 1529 (2013).
- [15] J. Błoczyński, X. G. Huang, X. Zhang, and J. Liao, *Nucl. Phys.* **A939**, 85 (2015).
- [16] X. G. Huang and J. Liao, *Phys. Rev. Lett.* **110**, 232302 (2013).
- [17] Y. Jiang, X. G. Huang, and J. Liao, *Phys. Rev. D* **91**, 045001 (2015).
- [18] S. Pu, S. Y. Wu, and D. L. Yang, *Phys. Rev. D* **91**, 025011 (2015).
- [19] K. Fukushima, D. E. Kharzeev, and H. J. Warringa, *Phys. Rev. D* **78**, 074033 (2008).
- [20] A. Yamamoto, *Phys. Rev. Lett.* **110**, 112001 (2013).
- [21] A. Yamamoto, *Eur. Phys. J. A* **57**, 211 (2021).
- [22] G. Endrodi and G. Marko, *Proc. Sci. LATTICE2021* (2022) 245.
- [23] G. Endrődi and G. Markó, *J. High Energy Phys.* **12** (2022) 015.
- [24] J. C. Yang, X. T. Chang, and J. X. Chen, *J. High Energy Phys.* **10** (2022) 053.
- [25] W. R. Tavares and S. S. Avancini, *Phys. Rev. D* **97**, 094001 (2018).
- [26] W. R. Tavares, R. L. S. Farias, and S. S. Avancini, *Phys. Rev. D* **101**, 016017 (2020).
- [27] G. Cao and X. G. Huang, *Phys. Rev. D* **93**, 016007 (2016).
- [28] M. Ruggieri, Z. Y. Lu, and G. X. Peng, *Phys. Rev. D* **94**, 116003 (2016).
- [29] M. Ruggieri and G. X. Peng, *Phys. Rev. D* **93**, 094021 (2016).
- [30] S. Klevansky and R. H. Lemmer, *Phys. Rev. D* **39**, 3478 (1989).
- [31] S. P. Klevansky, *Rev. Mod. Phys.* **64**, 649 (1992).
- [32] T. D. Cohen, D. A. McGady, and E. S. Werbos, *Phys. Rev. C* **76**, 055201 (2007).
- [33] B. C. Tiburzi, *Nucl. Phys.* **A814**, 74 (2008).
- [34] A. Ahmad, *Chin. Phys. C* **45**, 073109 (2021).
- [35] A. Ahmad and A. Farooq, arXiv:2302.13265.
- [36] M. Loewe, D. Valenzuela, and R. Zamora, *Phys. Rev. D* **105**, 036017 (2022).
- [37] M. Loewe, D. Valenzuela, and R. Zamora, arXiv:2207.12387.
- [38] M. Loewe and R. Zamora, *Phys. Rev. D* **105**, 076011 (2022).
- [39] J. O. Andersen, W. R. Naylor, and A. Tranberg, *Rev. Mod. Phys.* **88**, 025001 (2016).
- [40] V. Skokov, B. Friman, E. Nakano, K. Redlich, and B. J. Schaefer, *Phys. Rev. D* **82**, 034029 (2010).
- [41] A. Ayala, J. L. Hernández, L. Hernández, R. L. Farias, and R. Zamora, *Phys. Rev. D* **103**, 054038 (2021).
- [42] A. Ayala, R. L. S. Farias, S. Hernández-Ortiz, L. Hernández, D. M. Paret, and R. Zamora, *Phys. Rev. D* **98**, 114008 (2018).
- [43] A. Ayala, S. Hernández-Ortiz, and L. A. Hernández, *Rev. Mex. Fis.* **64**, 302 (2018).
- [44] J. S. Schwinger, *Phys. Rev.* **82**, 664 (1951).
- [45] J. W. L. Glaisher, *Messenger Math* **7**, 43 (1878).
- [46] R. L. Workman *et al.*, *Prog. Theor. Exp. Phys.* **2022**, 083C01 (2022).
- [47] H. Li, X. L. Sheng, and Q. Wang, *Phys. Rev. C* **94**, 044903 (2016).
- [48] N. Bilic and H. Nikolic, *Eur. Phys. J. C* **6**, 515 (1999).
- [49] A. Ayala, C. Dominguez, L. Hernández, M. Loewe, A. Raya, J. Rojas, and C. Villavicencio, *Phys. Rev. D* **94**, 054019 (2016).